AIMS Materials Science, 4(3): 582-593.
DOI: 10.3934/matersci.2017.3.582
Received: 28 December 2016
Accepted: 06 March 2017
Published: 05 May 2017

http://www.aimspress.com/journal/Materials

Research article

Characterizing the surface charge of clay minerals with Atomic Force Microscope (AFM)

Yuan Guo and Xiong (Bill) Yu *

Department of Civil Engineering, Case Western Reserve University, 2104 Adelbert Road, Cleveland, OH 44106, USA

* **Correspondence:** Email: xiong.yu@case.edu; Tel: +1-216-368-6247.

Abstract: The engineering properties of clayey soils, including fluid permeability, erosion resistance and cohesive strength, are quite different from those of non-cohesive soils. This is mainly due to their small platy particle shape and the surrounding diffuse double layer structure. By using the Atomic Force Microscopy (AFM), the surface topography and the interaction force between the silicon dioxide tip and the kaolinite/montmorillonite clay minerals have been measured in the 1.0 mM NaCl solution at neutral pH. From this, the surface potential of the clay minerals is determined by mathematical regression analyses using the DLVO model. The length/thickness ratio of kaolinite and montmorillonite particles measured ranges from 8.0 to 15.0. The surface potential and surface charge density vary with particles. The average surface potential of montmorillonite is −62.8 ± 10.6 mV, and the average surface potential of kaolinite is −40.9 ± 15.5 mV. The measured results help to understand the clay sediment interaction, and will be used to develop interparticle force model to simulate sediment transport during erosion process.

Keywords: AFM; kaolinite; montmorillonite; surface potential; DLVO model

1. Introduction

Clay minerals, including kaolinite, montmorillonite and illite, are hydrous aluminum silicates with layered structures and small sizes at the micron or submicron scale. Cohesive soils, or soils with high clay mineral content, have cohesive strength and show plasticity when moist. The engineering properties (e.g., fluid permeability, erosion resistance, cohesive strength, etc.) of cohesive soils are quite different from those of non-cohesive soils [1,2]. The main reason of these differences lies in the

small platy shape of clay minerals and the diffuse double layer structure surrounding them [3,4,5]. According to the DLVO model, the interaction forces between two charged small particles in an electrolyte mainly consist of two parts: the short-range van der Waals attraction and the long-range electrostatic repulsion [6–9]. Quantification of these forces will help to understand the formation of clay suspension and may also explain the different engineering behaviors of various clayey soils.

Hamaker theory can be used to explain the van der Waals interaction between two clay particles, and the Hamaker constant can be accurately approximated by the Lifshitz model based on clay minerology [10,11,12]. However the electrostatic force between clay minerals in an electrolyte is much more complicated as it is controlled by various factors, e.g., particle size, surface potential of the clay mineral, surrounding temperature, ion concentration, ion valence, dielectric constant of the electrolyte, etc. [13–16]. Experiments show the surface charge property of clay minerals varies with the solution pH value, and in return influences the coagulation of clay suspensions [17,18,19]. To better describe the clay mineral interaction in the particle level, a more accurate calibration of the surface electric properties (i.e., surface potential and surface charge density) of clay minerals is required.

The zeta potential of the colloid particles can be easily measured through the electrophoresis experiment [13,14]. However the direct measurement of surface potential is still challenging. The Atomic Force Microscope (AFM) has been used recently to characterize the surface topography of clay minerals on the substrate [20,21,22]. It is shown by proper calibration of tip stiffness, the tiny interaction forces (usually in a few nanonewtons) between tip and particles in electrolyte can be measured accurately [23–26]. Based on the DLVO theory, the surface potential or surface charge density of the colloid particles can be deduced through mathematical regression, and the results are found to be consistent with the zeta potential measurements as well as the experimental observations [27–30].

In this paper, the AFM test has been conducted on kaolinite and montmorillonite in order to characterize the surface property of these clay minerals in 1.0 mM NaCl solution at neutral pH. The length/thickness ratio of the clay minerals has been compared through surface mapping. The mathematical equation of electrostatic force between a sphere and a plane has been deduced, and was used in the fitting of the AFM results. Surface potential and surface charge density of kaolinite and montmorillonite under the test conditions are calculated. These results will be very useful in the future modeling of clayey soils at the particle scale.

2. Theoretical Model for Interaction Forces of AFM Tip and Clay Mineral

The AFM tip and the platy clay mineral can be simplified as a sphere-flat substrate system (Figure 1). A theoretical model for the interaction forces between a sphere and a flat substrate has been proposed based on the DLVO theory. Electrostatic force and van der Waals force are considered in this model. Surface potential and surface charge density of the clay minerals can be deduced through the fitting of the force-separation measurement.

2.1. Van der Waals Attraction

The van der Waals force between two close spherical particles is given by Hamaker [10] (see Eq. (1)). For the sphere-flat substrate system, the attraction force can be acquired by approaching R_2

to infinity. The nonretarded Hamaker constant is calculated by the Lifshitz theory [11,31], and $A_{132} = 6.088 \times 10^{-21}$ J for a silica-water-silica system [13].

$$F^v = -\frac{A_{132}R_1R_2}{6t^2(R_1+R_2)} \tag{1}$$

where, F^v is the van der Waals force, in N (negative represents attraction);

A_{132} is the total Hamaker constant for two macroscopic Phases 1 and Phase 2 interacting across a Medium 3, in J;

R_1, R_1 are the radius of two spherical particles, in m;

t is the separation between two particles, in m.

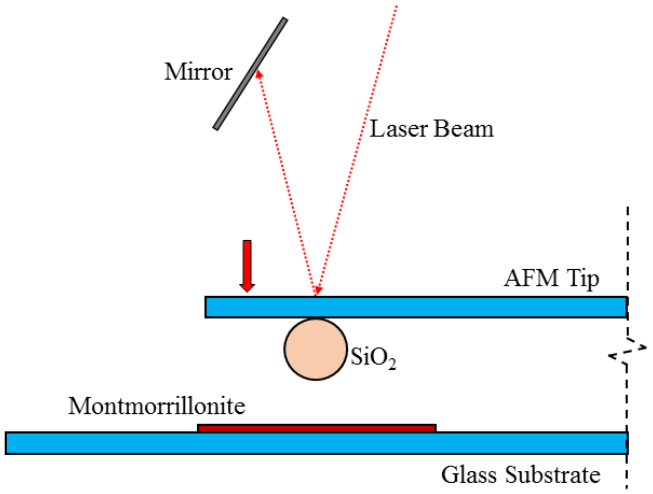

Figure 1. Schematic of AFM test of clay minerals under electrolyte.

2.2. Electrostatic Repulsion

The electrostatic force between a sphere and a flat substrate with different surface charge densities is deduced by integration. This method is also applicable to other complex-shaped AFM tips. The electrostatic force per unit area between two planar semi-infinite surfaces with low surface potentials (<25 mV) is provided in Eqs. (2) and (3) [32]. These equations have been used in the regression of surface electric property of clay minerals which may process a higher surface potential, and the potential deviation has been analyzed in details by comparing with other nonlinear approximations in the following section.

$$f = \frac{2}{\varepsilon_0\varepsilon_r}[\sigma_1\sigma_2 e^{-\kappa t} + (\sigma_1^2 + \sigma_2^2)e^{-2\kappa t}] \tag{2}$$

$$\kappa^{-1} = \left(\frac{\varepsilon_0\varepsilon_r kT}{2N_A M e^2}\right)^{\frac{1}{2}} \tag{3}$$

where, f is the electrostatic force per unit area, in N/m^2;

ε_0 is the vacuum permittivity, $\varepsilon_0 = 8.854 \times 10^{-12}$ C$^2 \cdot$ J$^{-1} \cdot$ m^{-1};

ε_r is the dielectric constant of the medium separating surfaces;
σ_1, σ_2 are the surface charge density of two surfaces, in C/m^2;
κ is the reciprocal of Debye length, in m^{-1};
t is the separation of two surfaces, in m;
k is the Boltzmann's constant, k = 1.381 × 10^{-23} J/K;
T is the temperature, in K;
e is the elementary charge, e = 1.602 × 10^{-19} C;
N_A is the Avogadro's number, N_A = 6.022 × 10^{23} mol^{-1};
M is the concentration of the electrolyte, in mol/m^3.

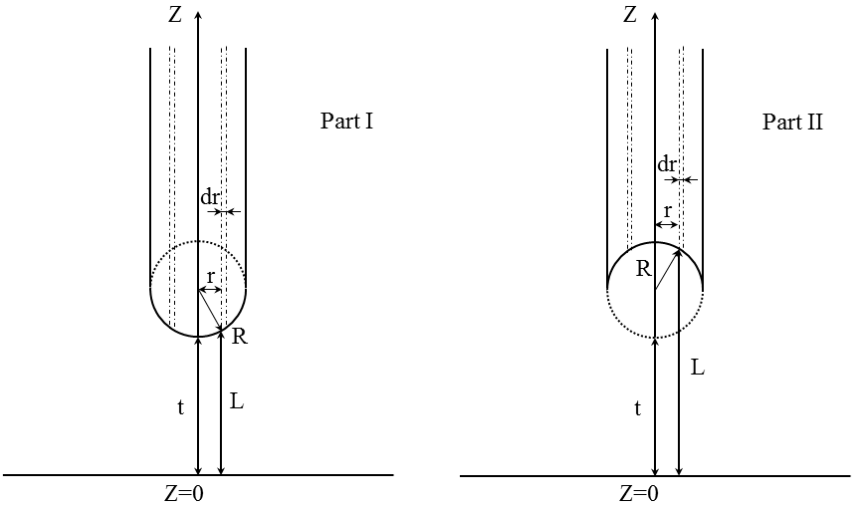

Figure 2. Geometry of the spherical tip-flat substrate system.

For the sphere-flat substrate system based on additivity, the total electrostatic force can be calculated by subtracting the interaction force of Part II from the interaction force of Part I (Figure 2). The electrostatic force of Part I or Part II is calculated by integration over the tip domain [28], as is given in Eq. (4).

$$F_{TS,I/II}^{e} = \int_0^R f \cdot 2\pi r dr \tag{4}$$

From the geometry of the spherical tip-flat substrate system, the following equations also stand:

$$R - \sqrt{R^2 - r^2} + t = L \text{ for Part I} \tag{5a}$$

$$R + \sqrt{R^2 - r^2} + t = L \text{ for Part II} \tag{5b}$$

where, r is the radius of the differential cylindrical surface, in m;
R is the radius of tip sphere, in m;
t is the separation distance between tip and surface, in m;
L is the distance between the bottom of differential surface and the flat surface, in m.

The final electrostatic force F^e between a sphere and a flat surface is given by Eq. (6).

$$\begin{aligned} F^e &= F^e_{TS,I} - F^e_{TS,II} \\ &= \frac{4\pi}{\varepsilon_0 \varepsilon_r \kappa^2} \sigma_1 \sigma_2 (\kappa R - 1)\left[e^{-\kappa t} - e^{-\kappa(t+2R)}\right] + \frac{2\pi}{\varepsilon_0 \varepsilon_r \kappa^2}(\sigma_1^2 \\ &\quad + \sigma_2^2)(\kappa R - 0.5)\left[e^{-2\kappa t} - e^{-2\kappa(t+2R)}\right] \end{aligned} \tag{6}$$

2.3. Total Interaction Force

The total interaction force between AFM tip and clay minerals equals to the sum of van der Waals attraction and electrostatic repulsion, as is shown in Eq. (7). The hydration force is not included here due to its relatively short acting range (less than a few nanometers).

$$F^{tot} = F^v + F^e \tag{7}$$

where, F^{tot} is the total interaction force between the AFM tip and the clay mineral;
F^v is the van der Waals attractive force;
F^e is the electrostatic repulsive force.

3. Materials and Method

Kaolinite sample and bentonite sample are provided by Georgia Kaolin Company and Wyo-Ben Inc. respectively. The kaolinite/montmorillonite suspensions were prepared by dissolving clay samples into highly purified water (with resistivity of 18.2 $\mathrm{M\Omega \cdot cm}$) to a concentration of 5,000 ppm and stirred for 1 hour. The suspensions were purified by passing the #200 sieve after stirring. No other chemical treatment was used. The well prepared suspension was dropped onto the glass slide and air-dried for 12 hours. During drying, the platy clay minerals will be adhered on the glass slide under fluid suction and remain fixed due to van der Waals attraction. The dry samples were washed with highly purified water for at least three times to remove the redundant clay minerals. Following the above steps, the kaolinite/montmorillonite minerals have been attached on the glass slide and will not dissolve into the electrolyte during the AFM test, providing reliable and accurate results.

The prepared samples were tested using the Veeco Dimension 3100 with the fluid cell module. The colloidal probes from Tipsnano OÜ were used to measure the interaction forces. Each probe has a spherical SiO_2 particle attached on the tip surface with a diameter of 0.9 μm (Figure 1). Product information provided by the manufacturer shows the size of the SiO_2 particle has a small deviation. The potential influence of particle size on the measured results will be further discussed in the subsequent section. Two different probes were used for the kaolinite and montmorillonite samples, and the calibrated tip stiffness is 0.76 N/m for the kaolinite sample and is 0.65 N/m for the montmorillonite sample. During the test, the surface topography was obtained through surface mapping before and after the force measurement in order to verify the testing spot. The 1.0 mM NaCl solution was used as the electrolyte and the pH is around 7.0. The clay minerals were immersed in the electrolyte for more than 10 min before the force measurement. The ambient temperature is kept to 20 ± 3 °C throughout the experiment. One notation is the clay minerals have a strong

heterogeneous surface charge distribution: at neutral pH, the minerals surface is negatively charged while the edge is positively charged [33,34]. In this study, the colloidal probes were used and all the measurements were conducted at the center of the clay samples, so that the fitting result can be regarded as an averaged surface electric property of clay minerals.

4. Results

The surface topography obtained before and after the force measurements showed little difference, and the clay minerals were fixed on the glass slide during the measurement and remained intact after the test. Through fitting to the mathematical model, the surface potential and surface charge density have been acquired and compared.

4.1. Surface Topography

The surface topography was scanned using the same colloidal tip before and after the force measurement in order to eliminate the concern of sample drifting during the experiment. It is shown the clay minerals were fixed on the glass slide and remain intact after the test. Two example measurements are shown in Figure 3. More than ten different samples for each type of clay minerals have been measured, and most of them are round or oval shaped. Due to the large size of the SiO_2 tip, the resolution of the mapping is lower than the regular tips. However, it is clear to see the platy structure of clay minerals (Figure 3), with the average length/thickness ratio of clay particles ranging from 8.0 to 15.0. Montmorillonite particles (0.8~3.0 μm) tend to be larger than kaolinite particles (0.4~1.2 μm).

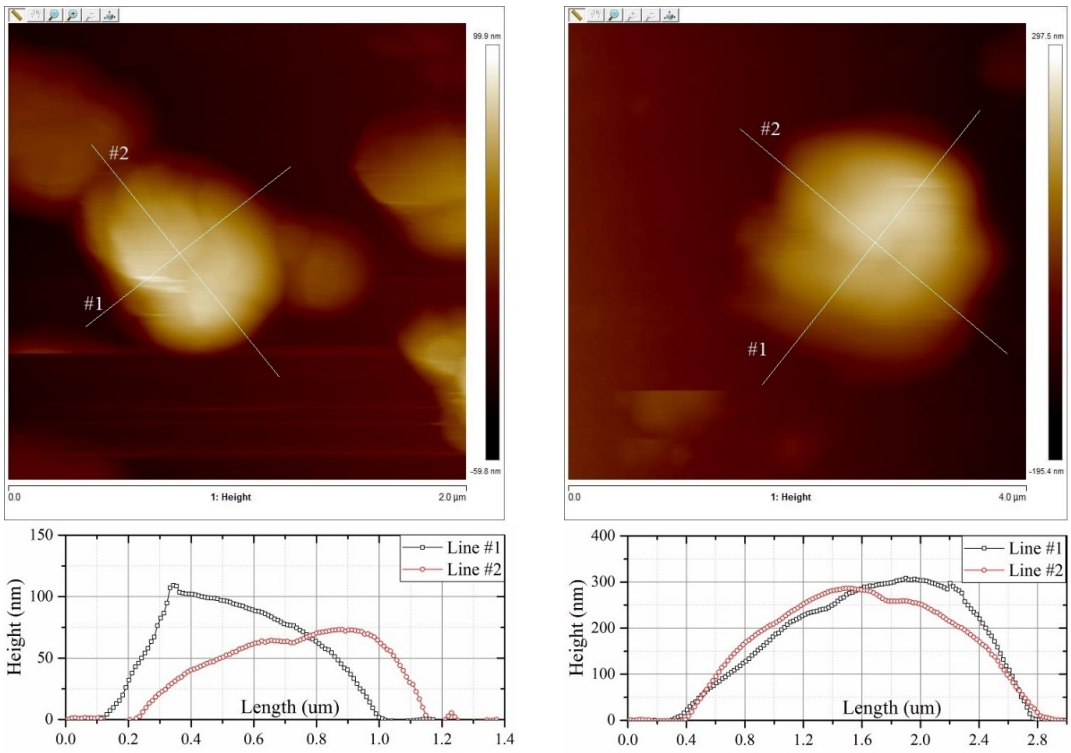

Figure 3. Surface topography of kaolinite (left) and montmorillonite (right).

4.2. Surface Charge Density and Surface Potential

The surface charge density of clay minerals has been acquired through fitting of the force-separation curve (Figure 4). A surface charge density of 0.005 C/m^2 was used for the SiO_2 tip under 1.0 mM NaCl electrolyte at pH = 7.0 [35,36,37]. The fitting practice shows the AFM test may not fully reflect the short-range attraction (<5 nm). However, the long-range electrostatic repulsion (>5 nm) can be measured accurately, which is the determinant factor in the regression process. The Debye length was also extracted from the logarithmic scale plot to serve as a validation of force measurement as is shown in Figure 4, and is highly consistent with the calculated value of 9.6 nm through Eq. (3).

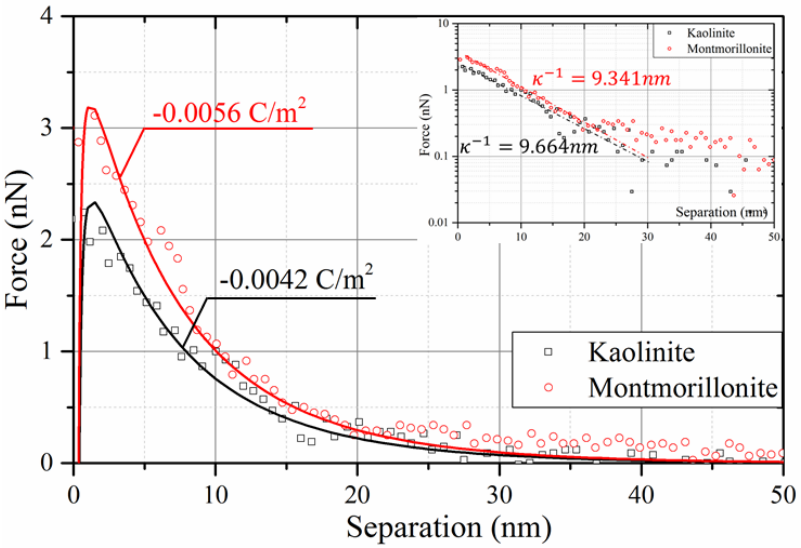

Figure 4. Fitting examples of interaction force between tip and clay minerals.

The surface potential of clay minerals was calculated from the surface charge density through the Grahame equation (Eq. (8)). For monovalent electrolyte (or 1–1 electrolyte), the surface charge density and the surface potential have the following relationship [13]:

$$\sigma = \sqrt{8\varepsilon_0\varepsilon_r kTN_A}\sinh\left(e\psi_0/2kT\right)M^{1/2} \tag{8}$$

where, σ is the surface charge density, in C/m^2;
ψ_0 is the surface potential, in V;
e is the elementary charge, $e = 1.602 \times 10^{-19}\ C$;
k is the Boltzmann's constant, $k = 1.381 \times 10^{-23}\ J/K$;
T is the absolute temperature, in K;
N_A is the Avogadro's number, $N_A = 6.022 \times 10^{23}\ mol^{-1}$;
M is the concentration of the electrolyte, in mol/m^3.

The fitting results are summarized in Table 1. The surface charge density of montmorillonite is about 1.7 times higher than that of kaolinite. It is also shown the surface potential and surface charge

density of clay minerals vary from particle to particle. The measured results of kaolinite show a higher deviation compared with montmorillonite, which may result from the different measuring faces of kaolinite. Some similar studies show the surface charge density of silica face of kaolinite is much higher than that of alumina face [38,39], while for montmorillonite both sides are silica surface. Kaolinite minerals prepared by this method may not have a strong face preference on which it adheres to the glass slide.

Table 1. Surface charge properties of clay minerals.

Clay Mineral	Surface Potential (mV)		Surface Charge Density (mC/m^2)	
	Mean	Standard Deviation	Mean	Standard Deviation
Kaolinite	−40.94	15.52	−3.50	1.53
Montmorillonite	−62.82	10.55	−6.03	1.52

4.3. Further Discussion

A few factors which may influence the accuracy of AFM measurement have been discussed in this section. The integration method used in the electrostatic interaction model is also applicable to other complex-shaped AFM tips. However it should be noted that Eq. (2) is proposed for low surface potential systems ($\psi < 25\ mV$) [32], and its accuracy for high surface potential clay minerals is underdetermined. To validate this model, the derived electrostatic force model has been compared with a nonlinear approximation proposed by Israelachvili as is given below [13].

$$F^e = \kappa RZe^{-\kappa t} \tag{9}$$

$$Z = 64\pi\varepsilon_0\varepsilon_r\left(\frac{kT}{e}\right)^2 tanh\left(\frac{ze\psi_1}{4kT}\right)tanh\left(\frac{ze\psi_2}{4kT}\right) \tag{10}$$

where, F^e is the electrostatic force between a plane and a sphere, in N;

κ^{-1} is the Debye length, in m;

R are the radius of spherical particle, in m;

Z is the interaction constant, in N;

ψ_1, ψ_2 are the surface potentials of sphere and plane, in V.

For a sphere-plane system (D = 900 nm) with surface potentials of −56 mV (SiO_2 sphere) and −63 mV (montmorillonite), it is shown although the peak interaction force in derived model is 29% higher than the nonlinear model, the difference of curvature at moderate separation (8 nm to 30 nm) is relatively smaller (averagely around 5%). Since the data fitting is mainly determined by the shape of the curvature at moderate separation rather than peak value, it is believed this simplified model could achieve relatively accurate fitting result for this study.

Product information provided by Tipsnano OÜ shows the dispersion of SiO_2 particle size on AFM tip is no more than 10%. The potential influence of SiO_2 particle size on the measured result has been analyzed here. The magnitude of interaction force between a plane and different sized particles (from diameter D = 850 nm to diameter D = 950 nm) is shown in Figure 5 (σ_1 = 0.005 C/m^2

& σ_2 = 0.0034 C/m^2), which could serve as the upper and lower boundaries of the potential deviation. As is given in Figure 5, for 850 nm and 950 nm spheres, the difference in the magnitude of peak interaction force is within 5.7%. The potential error due to inaccurate estimation of particle size should lie in this range. Another possible source of error may come from surface roughness of the SiO_2 sphere, which is not discussed in this paper. A SiO_2 sphere with a rough surface or a large bump may influence the measured force between tip and substrate. The SEM image of AFM tip provided by the manufacturer shows SiO_2 sphere has a high sphericity, and it is believed this influence can be small.

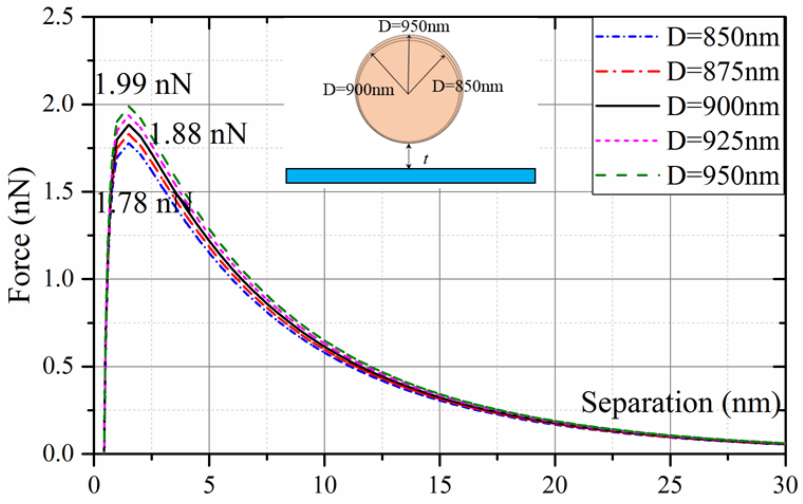

Figure 5. Interaction forces between platy plane and difference sized spheres.

5. Conclusion

The Atomic Force Microscope has been used to characterize the surface properties of kaolinite and montmorillonite under 1.0 mM NaCl electrolyte at neutral pH. The surface topography of two types of clay minerals and their non-contact forces with the spherical SiO_2 tip were measured during the test. A mathematical model describing the interaction force between the spherical AFM tip and the platy clay mineral was proposed and used in the mathematical fitting of surface electric properties, including surface charge density and surface potential. This method is also applicable to other complex-shaped AFM tips. The derived model was compared with Israelachvili's nonlinear approximation of electrical double layer force and showed a decent accuracy. The influence of size deviation of SiO_2 sphere on the force measurement has also been analyzed.

The results show both the kaolinite and the montmorillonite are platy shaped particles with the length/thickness ratio ranging from 8.0 to 15.0. Montmorillonite particles (0.8~3.0 μm) tend to be larger than the kaolinite particles (0.4~1.2 μm). The surface charge density and surface potential of the clay minerals vary from particle to particle, especially for the kaolinite which has two different silica and alumina faces. The average surface charge densities of montmorillonite and kaolinite are −6.03 ± 1.5 mC/m^2 and −3.5 ± 1.5 mC/m^2. The average surface potentials of montmorillonite and kaolinite are −62.8 ± 10.6 mV and −40.9 ± 15.5 mV, respectively. These results will be used in the future particle-scale modeling of clay suspension and clay sediment transport.

Acknowledgments

This research is partially supported by the US National Science Foundation via grant No. 0846475 and 0900401.

Conflict of Interest

The authors declare that there is no conflict of interest regarding the publication of this manuscript.

References

1. Terzaghi K (1943) *Theoretical soil mechanics*, New York: John Wiley & Sons, Inc.
2. Briaud JL, Chen HC, Li Y, et al. (2004) SRICOS-EFA method for complex piers in fine-grained soils. *J Geotech Geoenviron* 130: 1180–1191.
3. Lu N, Anandarajah A (1992) Empirical estimation of double-layer repulsive force between two inclined clay particles of finite length. *J Geotech Eng* 118: 628–634.
4. Katti DR, Matar MI, Katti KS, et al. (2009) Multiscale modeling of swelling clays: A computational and experimental approach. *KSCE J Civ Eng* 13: 243–255.
5. Bayesteh H, Mirghasemi AA (2015) Numerical simulation of porosity and tortuosity effect on the permeability in clay: microstructural approach. *Soils Found* 55: 1158–1170.
6. Derjaguin B, Landau L (1941) Theory of stability of strongly charged lyophobic sols and of the adhesion of strongly charged particles in solutions of electrolytes. *Acta Physicochem URSS* 14: 633–662.
7. Verwey EJW, Overbeek JTG (1948) *Theory of the stability of lyophobic colloids*, New York: Elsevier Publishing Company, Inc.
8. Anandarajah A (1994) Discrete element method for simulating behavior of cohesive soil. *J Geotech Eng* 120: 1593–1613.
9. Anderson MT, Lu N (2001) Role of microscopic physico-chemical forces in large volumetric strains for clay. *J Eng Mech* 127: 710–719.
10. Hamaker HC (1937) The London-van der Waals attraction between spherical particles. *Physica* 4: 1058–1072.
11. Lifshitz EM (1956) The theory of molecular attractive forces between solids. *Soviet Phys* 2: 73–83.
12. Bergstrom L (1997) Hamaker constants of inorganic materials. *Adv Colloid Interfac* 70: 125–169.
13. Israelachvili JN (2011) *Intermolecular and surface forces*, USA: Academic Press.
14. Rodriguez K, Araujo M (2006) Temperature and pressure effects on zeta potential values of reservoir minerals. *J Colloid Interf Sci* 300: 788–794.
15. Garcia-Garcia S, Jonsson M, Wold S (2006) Temperature effect on the stability of bentonite colloids in water. *J Colloid Interf Sci* 298: 694–705.
16. Lu N, Anderson MT, Likos WJ, et al. (2008) A Discrete Element Model for kaolinite aggregate formation during sedimentation. *Int J Numer Anal Met* 32: 965–980.
17. Kretzschmar R, Holthoff H, Sticher H (1998) Influence of pH and humic acid on coagulation kinetics of kaolinite: a dynamic light scattering study. *J Colloid Interf Sci* 202: 95–103.

18. Benna M, Kbir-Ariguib N, Magnin A, et al. (1999) Effect of pH on rheological properties of purified sodium bentonite suspensions. *J Colloid Interf Sci* 218: 442–455.
19. Gupta V, Hampton MA, Stokes JR, et al. (2011) Particle interactions in kaolinite suspensions and corresponding aggregate structures. *J Colloid Interf Sci* 359: 95–103.
20. Zhang M, Rong M, Zeng H, et al. (2001) Atomic force microscopy study on structure and properties of irradiation grafted silica particles in polypropylene-based nanocomposites. *J Appl Polym Sci* 80: 2218–2227.
21. Szabó T, Wang J, Volodin A, et al. (2009) AFM study of smectites in hybrid Langmuir-Blodgett films: saponite, wyoming bentonite, hectorite, and laponite. *Clay Clay Miner* 57: 706–714.
22. Firoozi AA, Taha MR, Firoozi AA, et al. (2015) Effect of ultrasonic treatment on clay microfabric evaluation by atomic force microscopy. *Measurement* 66: 244–252.
23. Veeramasuneni S, Yalamanchili MR, Miller JD (1996) Measurement of interaction forces between silica and a-alumina by atomic force microscopy. *J Colloid Interf Sci* 184: 594–600.
24. Raiteri R, Margesin B, Grattarola M (1998) An atomic force microscope estimation of the point of zero charge of silicon insulators. *Sensor Actuat B-Chem* 46: 126–132.
25. Drelich J, Long J, Xu Z, et al. (2006) Probing colloidal forces between a Si_3N_4 AFM tip and single nanoparticles of silica and alumina. *J Colloid Interf Sci* 303: 627–638.
26. Huang Q, Wu H, Cai P, et al. (2015) Atomic force microscopy measurements of bacterial adhesion and biofilm formation onto clay-sized particles. *Sci Rep* 5: 16857.
27. Sokolov I, Ong QK, Shodiev H, et al. (2006) AFM study of forces between silica, silicon nitride and polyurethane pads. *J Colloid Interf Sci* 300: 475–481.
28. Drelich J, Jun L, Anthony Y (2007) Determining surface potential of the bitumen-water interface at nanoscale resolution using atomic force microscopy. *Can J Chem Eng* 85: 625–634.
29. Liu J, Sandaklie-Nikolova L, Wang X, et al. (2014) Surface force measurements at kaolinite edge surfaces using atomic force microscopy. *J Colloid Interf Sci* 420: 35–40.
30. Dobryden I, Potapova E, Holmgren A, et al. (2015) Force interactions between magnetite, silica, and bentonite studied with atomic force microscopy. *Phys Chem Miner* 42: 319–326.
31. Ninham BW, Parsegian VA (1970) Van der Waals forces: special characteristics in lipid-water systems and a general method of calculation based on the Lifshitz theory. *Biophys J* 10: 646–663.
32. Parsegian VA, Gingell D (1972) On the electrostatic interaction across a salt solution between two bodies bearing unequal charges. *Biophys J* 12: 1192–1204.
33. Liu J, Gaikwad R, Hande A, et al. (2015). Mapping and Quantifying Surface Charges on Clay Nanoparticles. *Langmuir* 31: 10469–10476.
34. Brady PV, Cygan RT, Nagy K (1996) Molecular Controls on Kaolinite Surface Charge. *J Colloid Interf Sci* 183: 356–364.
35. Kosmulski M (2001) *Chemcal properties of material surfaces*, New York: Marcel Dekker, Inc.
36. Barhoumi H, Maaref A, Jaffrezic-Renault N (2010) Experimental study of thermodynamic surface characteristics and pH sensitivity of silicon dioxide and silicon nitride. *Langmuir* 26: 7165–7173.
37. Barisik M, Atalay S, Beskok A, et al. (2014) Size dependent surface charge properties of silica nanoparticles. *J Phys Chem C* 118: 1836–1842.
38. Gupta V, Miller JD (2010) Surface force measurements at the basal planes of ordered kaolinite particles. *J Colloid Interf Sci* 344: 362–371.

39. Kumar N, Zhao C, Klaassen A, et al. (2016) Characterization of the surface charge distribution on kaolinite particles using high resolution atomic force microscopy. *Geochim Cosmochim Ac* 175: 100–112.